33RD CONGRESS
OF THE INTERNATIONAL COUNCIL
OF THE AERONAUTICAL SCIENCES
STOCKHOLM, SWEDEN, 4-9 SEPTEMBER, 2022

ICAS 2022 SWEDEN

TRANSITIONAL FLOW MODELLING OF A HYBRID LAMINAR FLOW CONTROL AND VARIABLE CAMBER TRANSONIC TRANSPORT AIRCRAFT WING

Mauricio M. Jentys[1] & Christian Breitsamter[1]

[1]Chair of Aerodynamics and Fluid Mechanics, Technical University of Munich , Boltzmannstraße 15, 85748 Garching, Germany

Abstract

This paper presents computational fluid dynamics (CFD) results of the transitional flow field around a transonic transport aircraft wing. The framework for the analyses is formed by the german LuFo VI-1 project CATeW (*Coupled Aerodynamic Technologies for Aircraft Wings*), where benefits of the technology coupling between a hybrid laminar flow control (HLFC) system and a variable camber (VC) wing on aerodynamic drag is assessed. The computational fluid dynamics framework for the modelling of both technologies is presented in the paper, followed by CFD results considering a variation in both suction strength and deflection angle of an Adaptive Dropped Hinge Flap (ADHF), the latter integrating the VC capability to the aircraft wing. Transition prediction is performed following two strategies; on the one hand, the $\gamma - Re_\theta + CF$ turbulence model is applied, predicting an overall drag reduction with suitable suction and deflection angle settings reflecting the downstream shift of the transition location with increasing suction strength. On the other hand, linear stability theory with a two-N-factor integration strategy for transition prediction is applied. This allows for a quantitative assessment of targeted synergy effects between the coupled HLFC and VC application, namely suppression of Tollmien-Schlichting instabilities through a favorable adaptation of the wing's surface pressure distribution downstream of the HLFC suction panel. A reduction in N-factors is reflected for adapted deflection angles of the ADHF, indicating the synergy potential of the presented HLFC-VC coupling. As a last step, predicted transition location of both methods are compared, showing accordance in predicting transition in direct vicinity of the wing's leading edge for large sections of the wing's span for the no suction case. Generally, the transition location of the two-N-factor method lies upstream with respect to the location of the $\gamma - Re_\theta + CF$ model. Differences arise in the outboard section of the wing's suction side, where the two-N-factor method predicts a change in transition mechanism to critical amplification of Tollmien-Schlichting waves for the chosen critical N-factors.

Keywords: Hybrid Laminar Flow Control, Variable Camber, Drag Reduction, CFD, Transition Prediction

1. Introduction

Fuel efficiency is a driving factor during development of next generation transport aircraft. Not only does this provide for performance and thus economic benefits, but major advances in fuel efficiency are necessary to cope with environmental requirements, formulated for instance by the ACARE in their Flightpath 2050 report [1].

Different aerodynamic drag reduction techniques have been intensively investigated in the past, from which two of the most promising candidates are hybrid laminar flow control (HLFC) and variable camber (VC) systems. On an individual basis the potential for drag reduction has been assessed, regarding HLFC for instance in Ref. [2] or Ref. [3] and VC in Ref. [4] and Ref. [5]. Their coupled application, however, is still an open research question and might offer even higher potential for drag reduction due to synergy effects, as indicated in Fig. 1 and Sec. 2.

Investigating the potential for drag reduction and aerodynamic interaction effects between a coupled HLFC-VC application motivated the LuFo VI-1 project CATeW (*Coupled Aerodynamic Technologies*

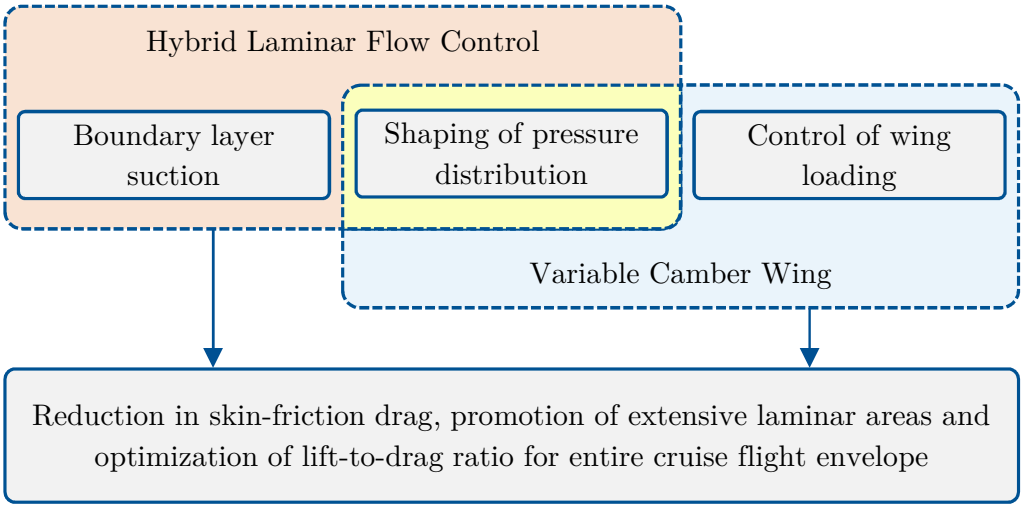

Figure 1 – Schematic representation of individual HLFC and VC integration and synergetic overlap.

for Aircraft Wings), which forms the framework for the contribution at hand.
CATeW is a joint project between the Institute of Aerospace Systems (ILR) of RWTH Aachen University and the Chair of Aerodynamics and Fluid Mechanics (AER) of the Technical University of Munich. To gain detailed insight into aerodynamic interaction effects when simultaneously operating both systems on a transonic transport aircraft wing, high-fidelity (HiFi) analyses by means of computational fluid dynamics (CFD) are performed at AER within the scope of CATeW, while an assessment on system level is achieved using the overall aircraft design (OAD) toolchain MICADO [6, 7] at ILR. Furthermore, incorporation of HiFi-analyses' results into MICADO by means of reduced order models is intended.
The scope of this contribution lies on the presentation of the HiFi-CFD toolchain for transitional flow modelling of the technology coupling, alongside results applying the $\gamma - Re_\theta + CF$ transition turbulence model and the linear stability theory based two-N-factor strategy for transition prediction for the wing flow of the project's reference configuration CATeW-02. This allows for a comparison between both transition prediction modelling approaches, while the linear stability analyses provide further insight into the different critical transition mechanisms and synergy effects of VC application with regard to suppressing boundary layer transition. The paper is organized as follows:

Sec. 2.: Introduction to fundamentals considering laminar-turbulent boundary layer transition, alongside an introduction to the expected benefits of a combined HLFC and VC application

Sec. 3.: Presentation of the applied CFD framework:

- Geometry of the reference configuration's wing, derived for turbulent boundary layer flow
- Modelling approach implemented in the course of CATeW for HLFC and VC in the CFD context
- Methodologies for transition prediction applied within this contribution

Sec. 4.: Results for the reference configuration CATeW-02

Sec. 5.: Conclusions and outlook

A complementary conference contribution focusing on the LowFi side of the project, including latest developments in MICADO for modelling of the technology coupling and results for the reference configuration is presented by Effing et. al in Ref. [8].

2. Fundamentals

This section provides a short overview regarding primary mechanisms for boundary layer transition on swept, tapered aircraft wings. Furthermore, HLFC as a tool to delay boundary layer transition and its coupling effects with VC are briefly discussed.

Boundary Layer Transition

Boundary layer transition is affected by multiple parameters, with the most dominant being the Reynolds number, surface roughness, turbulence intensity and the external flow's pressure distribution. For an exhaustive overview the reader may refer to Ref. [9]

Considering tapered, swept aircraft wings three primary instability mechanisms are of central interest, namely transition due to Tollmien-Schlichting instabilities (TSI), cross-flow instabilities (CFI) and attachment line transition (ALT). A sketch representing the predominant areas of occurrence on an aircraft wing is shown in Fig. 2. Transition due to TSI is the main transition mechanism in two-

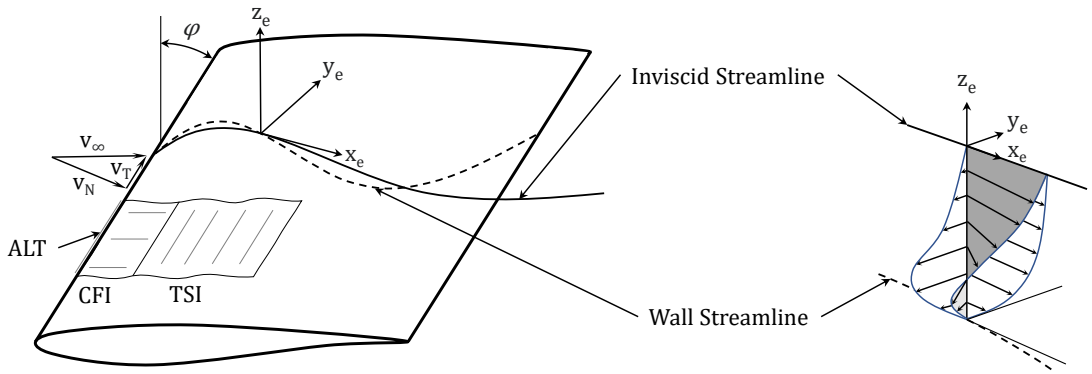

Figure 2 – Primary instability mechanisms on a swept aircraft wing, alongside a visualization of the three-dimensional boundary layer development (adapted from Refs. [10, 11]). The subscript e denotes a cartesian coordinate system aligned with its x-direction along the inviscid streamline at the boundary layer's edge, z points in wall normal direction and y in the corresponding cross-flow direction.

dimensional flows, thus typically triggering boundary layer transition on unswept or slightly swept wings ($\varphi \leq 25°$). For higher sweep angles, provided neither ALT or CFI mechanisms trigger transition, the critical region for transition due to TSI is typically located mid-chord, downstream of the point of minimum pressure. An effective mean of stabilization for Tollmien-Schlichting waves is assuring a proverse (negative) pressure gradient along the flow direction [6].

The main transition mechanism for wings with leading edge sweep angles $\varphi > 25°$ is represented by CFI. This type of instability is mainly found in direct vicinity of the wing's leading edge, where strong pressure gradients perpendicular to the streamlines lead to the development of a cross-flow velocity profile throughout the boundary layer (Fig. 2, right). Due to the cross-flow velocity being zero both at the wall and the edge of the boundary layer (Fig. 2, subscript e), the cross-flow velocity profile features an inflection point, which inherently presents a sufficient condition for (inviscid) instability [9, 12].

The third critical transition mechanism is the attachment line transition (ALT). This transition mechanism causes the boundary layer around a wing to be entirely turbulent, and is typically caused by so-called leading edge contamination (LEC). LEC arises through the propagation of disturbances from the turbulent boundary layer of the fuselage along the wing's leading edge. Apart from that, the attachment line is susceptible itself to instabilities causing transition. A criterion based on the attachment-line momentum-thickness Reynolds number $Re_{\theta,AL} < Re_{\theta,AL,crit}$ formulated by Pfenninger [13] and experimentally confirmed by Poll [14] is usually applied to evaluate the occurrence of ALT [6, 9].

Hybrid Laminar Flow Control and Variable Camber Technology

HLFC primarily aims at delaying boundary layer transition through the above presented mechanisms, thus reducing the wing's skin friction drag $C_{D,f}$ by maintaining extended areas of laminar flow. Considering an aircraft wing, the term "hybrid" thereby stems from the combination of an active boundary layer suction system (LFC, laminar flow control) in the wing's leading edge region, coupled with passive means of natural laminar flow (NLF) in the wing mid chord region. While in the case of highly swept aircraft wings active boundary layer suction is necessary to suppress transition due to CFI and possibly ALT, an appropriate choice of airfoil and wing geometry as a mean of NLF typically suffices to suppress transition due to TSI. This is related to a favorable shaping of the wing streamwise surface pressure distribution and especially its gradient ($\partial p/\partial x < 0$) stabilizing laminar boundary layers in terms of TSI [6, 9].

Considering a transport aircraft, airfoil and wing geometry are optimized for a specific design point, namely the design lift coefficient C_L. However, a typical transport aircraft's mission is characterized by large sections of the aircraft flying in off-design conditions, due to air traffic restrictions prohibiting a continuous climb pattern with constant lift coefficient [15]. The typically resulting step climb procedure and associated off-design mission segments in return mean, geometry adaptation through VC integration not only presenting a possibility to improve lift-to-drag ratio for off-design mission segments, but at the same time acting as an enabler to optimize the NLF component of the HLFC system through adaptation of the surface pressure distribution for the latter segments.

3. Computational Fluid Dynamics Framework

The CFD simulations presented within this paper are performed with the DLR TAU Code [16]. The TAU Code is an unstructured, three-dimensional finite volume solver incorporating an edge-based dual-cell approach. For the computations in this publication, a second order central scheme is applied for discretization of inviscid fluxes and viscous terms. As the observed cases are steady, an implicit local time stepping technique is applied in all computations.

An overview of the reference wing CATeW-02 is presented in Sec. 3.1, along with an overview of the computational mesh applied for the analyses. A brief summary of techniques applied for HLFC and VC modelling in the CFD context is given in Sec. 3.2, followed by an introduction of different transition prediction techniques applied in the context of this paper, see Sec. 3.3.

3.1 Reference Geometry and Computational Grid

The wing geometry investigated within this paper is extracted from the project's reference configuration CATeW-02. The reference configuration CATeW-02 is based on the AVACON research baseline 2028 [17] and has been derived at ILR, encompassing a mid-range mission with fully turbulent wing flow. In comparison to the reference CATeW-01, as presented in Ref. [18], CATeW-02 presents an updated geometry iteration incorporating a different root airfoil (A1, Fig. 3). A planform view, key geometric and mission figures and an indication of HLFC and VC integration is given in Tab. 1 and Fig. 3. As presented in Fig. 3, VC integration is foreseen by deflections of an Adaptive Dropped Hinge Flap (ADHF) [19, 20], thus utilizing its multi-functional character beyond the primary purpose of a high-lift system.

Computational grids for CATeW-02 are generated using the commercial grid generator CENTAUR by CentaurSoft. Grids are generated in an unstructured manner, where the boundary layer is resolved by a prismatic layer with a stack height of 60 and an expansion ratio of 1.1. The dimensionless wall distance satisfies $y^+ < 1.0$ on all wall-boundaries, the wing contour is resolved with approximately 200 grid points in streamwise direction. The grids are generated following the studies and best practice guidelines for application of transition turbulence models presented in Ref. [21]. The resulting grid after performing an independence study consists of approximately $55 \cdot 10^6$ elements, an overview is given in Fig. 4.

Table 1 – Main mission and geometrical parameters of the reference configuration CATeW-01.

Mission Parameters	
Design range $\mathrm{R_D}$	4600 NM
Cruise Mach number $\mathrm{Ma_{cr}}$	0.83
Initial cruise altitude ICA	35000 ft
Cruise C_L	0.5 ± 0.05
Geometrical Parameters	
Wing reference area S_{ref}	220.2 m^2
Wing span b	52 m
Mean aerodynamic chord c_{ref}	5.29 m
Aspect ratio Λ	12.28
LE sweep φ_{LE}	33.43°
TE sweep φ_{TE}	26.01°
ADHF Parameters	IB / OB
Flap limit positions η_{F}	0.31 / 0.68
Relative chordlength $c_{\mathrm{ADHF}}/c_{\mathrm{loc}}$	0.3 / 0.3
Relative hinge position $x_{\mathrm{H}}/c_{\mathrm{loc}}$	0.747 / 0.708
Relative hinge position $z_{\mathrm{H}}/c_{\mathrm{loc}}$	-0.097 / -0.112

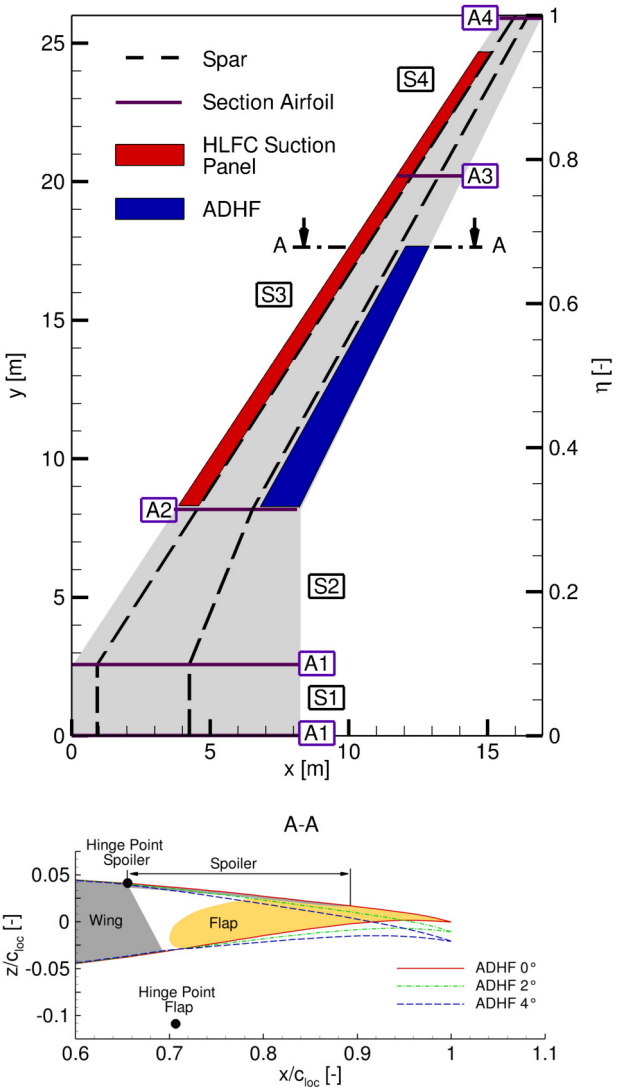

Figure 3 – CATeW-02 planform with indication of HLFC suction panel and VC integration through the ADHF system, adapted from [18].

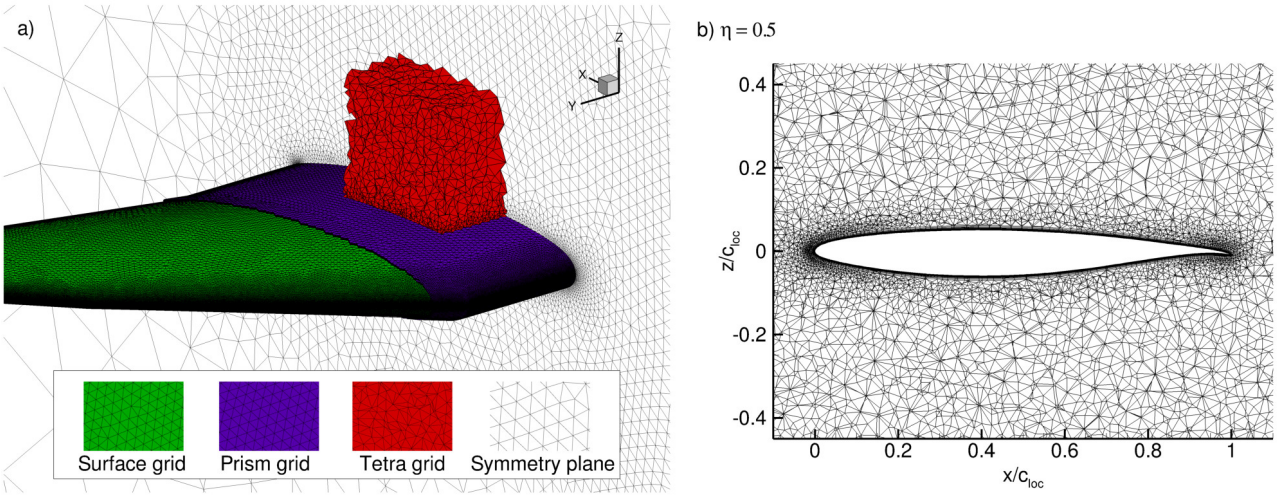

Figure 4 – a) Overview of general grid structure for CATeW-02. b) Cut through the volume mesh at a spanwise position of $\eta = 0.5$.

3.2 Modelling of HLFC and VC

To model the technology coupling in context of CFD simulations, a modular python environment communicating mainly via file I/O with the required modules of the DLR TAU code is being implemented in the course of CATeW. An overview over the different modules and their interdependencies is presented in Fig. 5.
The BuildWing module forms the main module of the CATeW Python environment. Since geometrical data from the project partner's OAD tool MICADO is stored and communicated in a so-called AiX (Aircraft Exchange) XML file, the BuildWing module generates a parameterized, three-dimensional wing geometry in terms of associated point clouds alongside python objects containing key geometrical parameters for subsequent modules. These geometry objects can either be passed to CAD software for generation of three-dimensional geometries for meshing, or as depicted in Fig. 5, to the subsequent ApplySuctionDist and Deformation modules.
In order to account for suction in the CFD simulations, an effusion mass flux boundary condition implemented for viscous walls within TAU, is applied [22, 23]. A wall-normal velocity is implemented through node-wise specification of the mass flux j per unit area, according to:

$$j = \frac{\dot{m}}{A} = V_n \cdot \rho \tag{1}$$

Using the parameterized wing geometry of the BuildWing module, the ApplySuctionDist module computes user-defined wall normal velocity distributions V_n in spanwise sections. These velocity distributions are transferred via radial basis function interpolation onto the unstructured CFD surface mesh. In the context of HLFC application, the suction strength is typically determined in terms of the suction coefficient C_q [6]:

$$C_q = \frac{V_n}{U_\infty} = \frac{j}{\rho \cdot U_\infty}, \tag{2}$$

which couples the node-wise prescription of wall-normal velocity V_n through the effusion mass-flux j to the local density ρ. Since the node-wise density ρ depends on the converged flow solution, a matching algorithm (see Fig. 5) is implemented within the ApplySuctionDist module, iteratively updating the prescribed effusion mass flux j with the converged density distribution to match the prescribed wall normal velocity V_n.

VC integration to the reference wing CATeW-02 is performed via the Deformation module. Again using the parameterized wing geometry of the BuildWing module, deflection fields according to the ADHF kinematic are computed. The ADHF kinematic features a Fowler-motion of the flap, accompanied

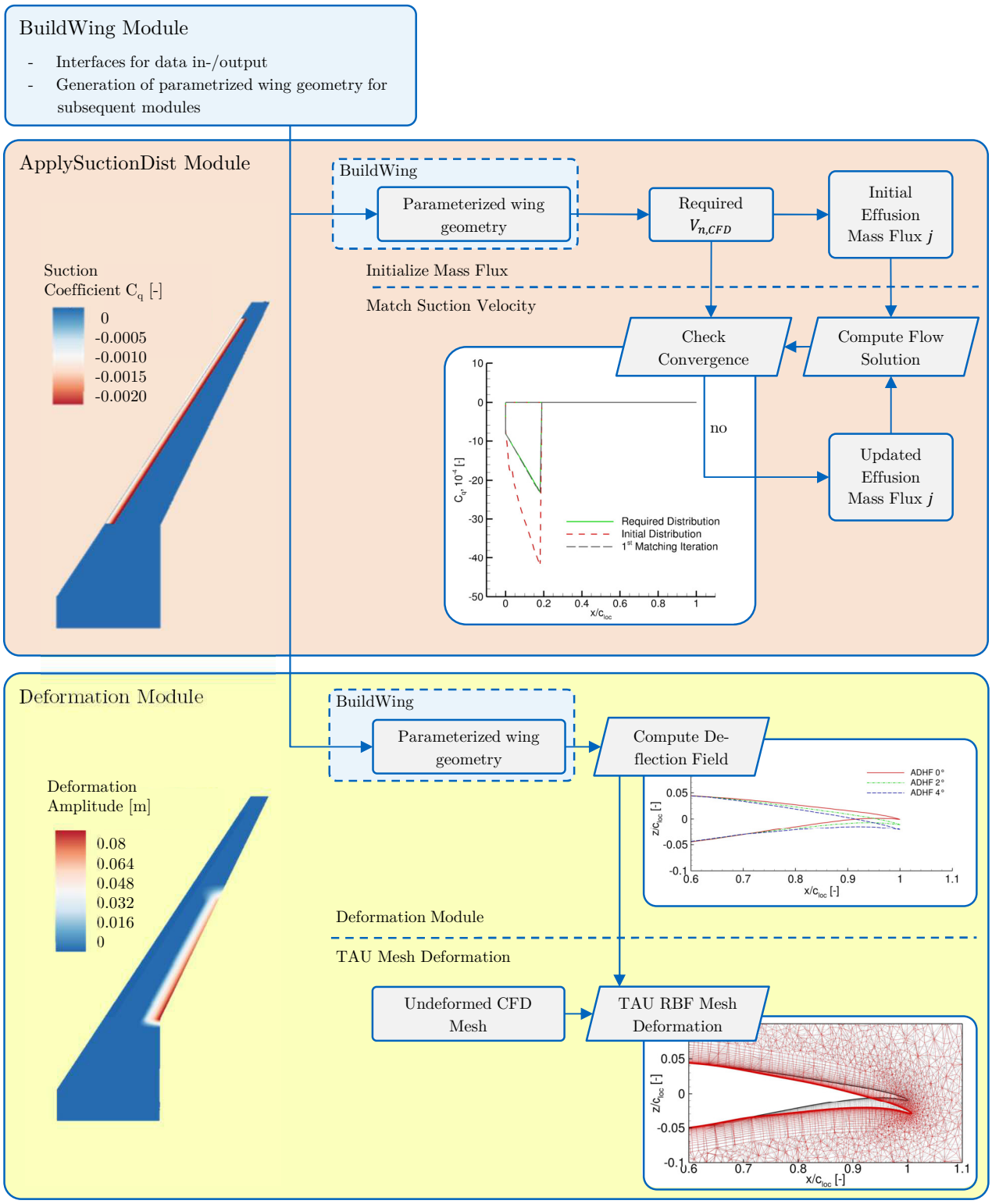

Figure 5 – Python environment implemented for simulation of the HLFC-VC technology coupling in CFD-computations.

by a spoiler droop to maintain a gap-free surface on the wing's suction side, see Fig. 3 bottom. The computed deflection fields are passed to TAU's mesh deformation routine, which interpolates the computed deflection fields via radial basis functions onto all grid points of the CFD volume mesh for an according deformation, see Fig. 5 bottom.

3.3 Transition Prediction

For transition prediction within this contribution, two different approaches are followed. Both methods are applicable for transition prediction due to TSI and CFI and are shortly introduced in the following.

Correlation-Based Transition Turbulence Model
A lot of effort is currently directed into the research of transition prediction within unstructured, parallel RANS solvers, within the framework of turbulence modelling. Within this paper, the $\gamma - Re_\theta + CF$ model, as presented in Ref. [24] and implemented within TAU is applied.
The $\gamma - Re_\theta + CF$ model is based on the model introduced by Langtry et. al in Ref. [25]. While the original model is only capable of predicting transition due to two-dimensional effects like TSI, the model presented by Grabe et. al in Ref. [24] has been extended for the effects of transition due to three-dimensional effects such as CFI.
The $\gamma - Re_\theta + CF$ model is based on the $k-\omega$ SST model [26] and solves two additional transport equations for the intermittency γ and the transition onset momentum thickness Reynolds number $Re_{\theta,t}$. For consideration of the cross-flow velocity profile, the helicity Reynolds number Re_{He} is computed in addition. For transition prediction, ratios depending on both Reynolds numbers are locally evaluated, which trigger a production term in the intermittency transport equation when reaching a critical value. The intermittency variable itself represents the flow state in the respective cells, with values of $\gamma = 1$ corresponding to fully turbulent and $\gamma = 0$ to laminar flow. To account for either a laminar or turbulent cell state in the computation, coupling to the $k-\omega$ SST model is achieved through an adaptation of the production and dissipation terms in the turbulent kinetic energy transport equation, primarily suppressing turbulent kinetic energy production in laminar cells. For an exhaustive overview of correlation based transition-transport models, especially with regard to the herein applied cross-flow extension, the reader may refer to Refs. [21, 24, 25].

Linear Stability Theory and two-N-factor Method
As a complementary tool for transition prediction, the linear stability theory (LST) solver LILO [27] with boundary layer profiles computed by COCO [28] is applied within this paper. LILO and COCO are coupled to TAU within an automated transition prediction module, see Ref. [29].
Within this contribution, COCO is applied along 22 line-in-flight cuts ($y = konst.$) along the wing's span. COCO computes compressible conical laminar boundary layer profiles from c_p-distributions extracted from the RANS solution. Using these boundary layer profiles, LILO performs a linear stability analysis following a two-N-factor strategy, namely by prescribed frequency/direction integration for derivation of Tollmien-Schlichting N-factors, and prescribed frequency/wavelength integration for cross-flow N-factors. Comparison with user-defined critical N-factors $N_{CF,crit}$ and $N_{TS,crit}$ yields the transition location to be iteratively applied to the RANS solver [6, 23]. For the turbulent part of the flow, the $k-\omega$ SST model [26] is applied in this paper.
Since critical N-factors are typically calibrated using wind-tunnel or flight tests, different critical N-factors are studied within this contribution. A summary is presented in Tab. 2, the derivation of the critical N-factors is based on Ref. [23] where N-factor calibrations have been performed with respect to wind-tunnel measurements of the CRM-NLF wing [30].

Table 2 – Critical N-factors chosen for two-N-factor transition prediction, according to [23].

	$N_{CF,crit}$	$N_{TS,crit}$
Upper limit	6.5	14
Average	6.0	12
Lower Limit	5.5	10

4. Results

The results presented in this contribution are computed for a cruise Mach number of $Ma_{cr} = 0.83$ and the initial cruise altitude of $ICA = 35.000$ ft, resulting in a Reynolds number of $Re_{cr} = 34.2 \cdot 10^6$ based on the wing's mean aerodynamic chord of $c_{ref} = 5.29$ m. The simulations use a target-C_L algorithm, where the angle of attack α is iteratively adapted to match the prescribed cruise lift coefficient of $C_L = 0.5$. The cases presented within this contribution encompass ADHF deflection angles of $\delta_{ADHF} = 0°, 2°$ and $4°$ and constant suction coefficients in the range of $C_q = [0; -24 \cdot 10^{-4}]$.

4.1 Correlation-Based Transition Turbulence Model

Using the above presented simulation framework (see Fig. 5), the influence of parameter variations in C_q and δ_{ADHF} on the wing's drag coefficient C_D are presented in Fig. 6, with a split into pressure drag $C_{D,p}$ and friction drag $C_{D,f}$ components following normal and tangential force integration on the wing surface.

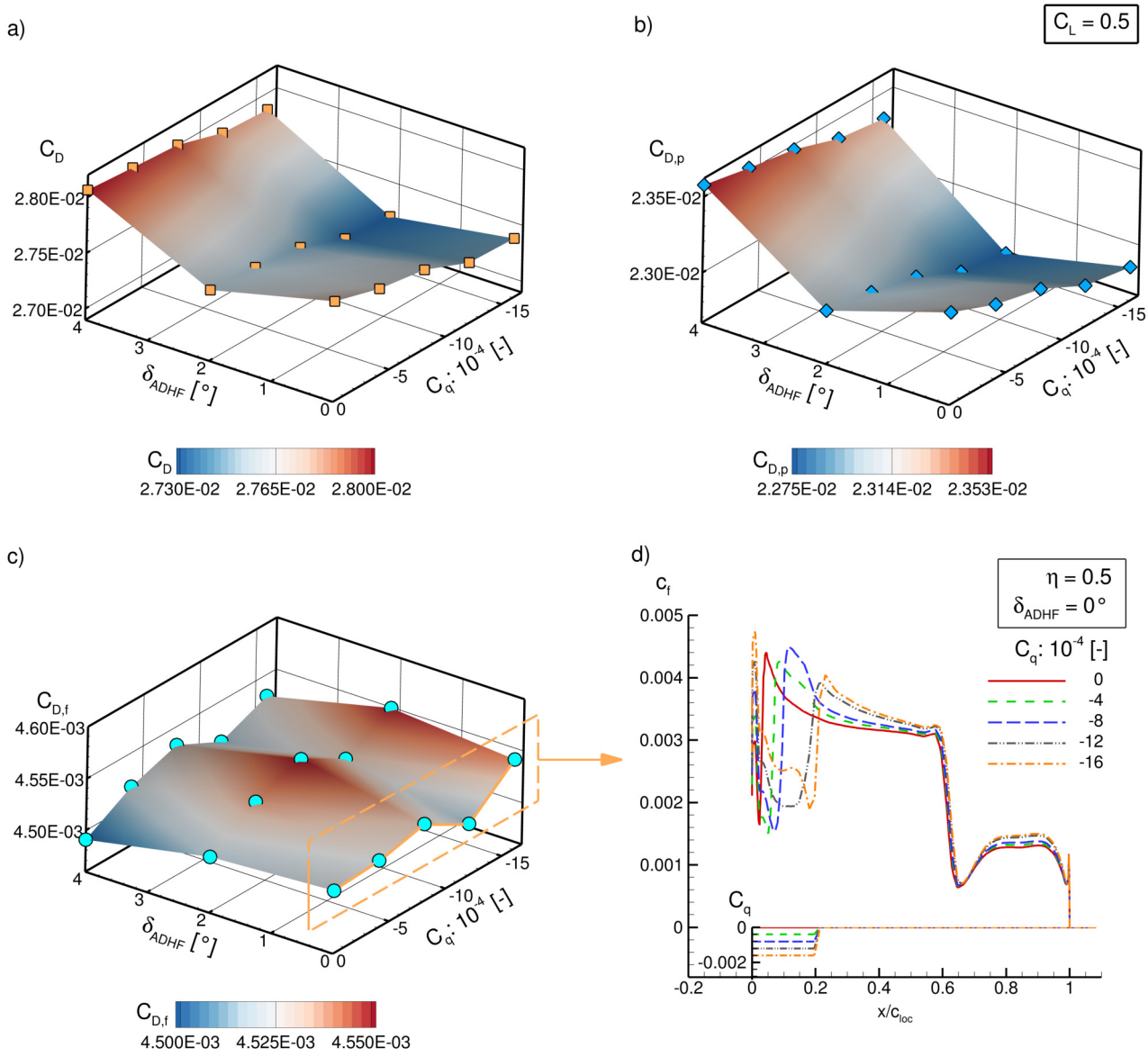

Figure 6 – Drag analysis for variations in ADHF deflection angle δ_{ADHF} and suction coefficient C_q for $C_L = 0.5$: a) Wing drag coefficient C_D, b) Pressure drag contribution $C_{D,p}$, c) Friction drag contribution $C_{D,f}$, d) Local skin friction coefficient c_f for $\delta_{ADHF} = 0°$, η = 0.5

As indicated in Fig. 6, a reduction in C_D is achieved when increasing the suction coefficient C_q, while the lowest overall drag coefficient is observable for an ADHF deflection of $\delta_{ADHF} = 2°$.
The drag reduction for the presented parameter range can be attributed to a reduction in pressure drag components, see Fig. 6 b), where the trend presented in the overall drag coefficient development is reflected correspondingly. Pressure drag reduction due to an increase in suction coefficient C_j can be attributed to a reduction in boundary layer thickness, stemming from the effect of suction itself on the one hand, and the delay in transition increasing the extent of a thinner boundary layer downstream of the suction panel on the other hand. This secondary effect of drag reduction is further promoted by suitable ADHF deflections.
Considering the development of the skin friction drag component $C_{D,f}$, only a small sensitivity to the parameter variations is observable for the configuration CATeW-02, see Fig. 6 c). The transition location is predicted to be successively shifted downstream with increasing suction strength, reaching the furthest downstream position for $C_q = -12 \cdot 10^{-4}$, see Fig. 7. The transition location corresponds to the streamwise limit of the HLFC suction panel for the main part of the wing span, in the spanwise region of $\eta \approx 0.85 - 0.95$ laminar flow extends downstream of the suction panel to a maximal chordwise station of $x_t/c_{loc} \approx 0.5$ at $\eta = 0.94$. With a further increase in suction strength above $C_q = -12 \cdot 10^{-4}$, the transition location is not predicted to be significantly shifted further downstream, see Fig 7.
Since the extent of laminar flow predicted for the wing of the configuration CATeW-02 is limited, the

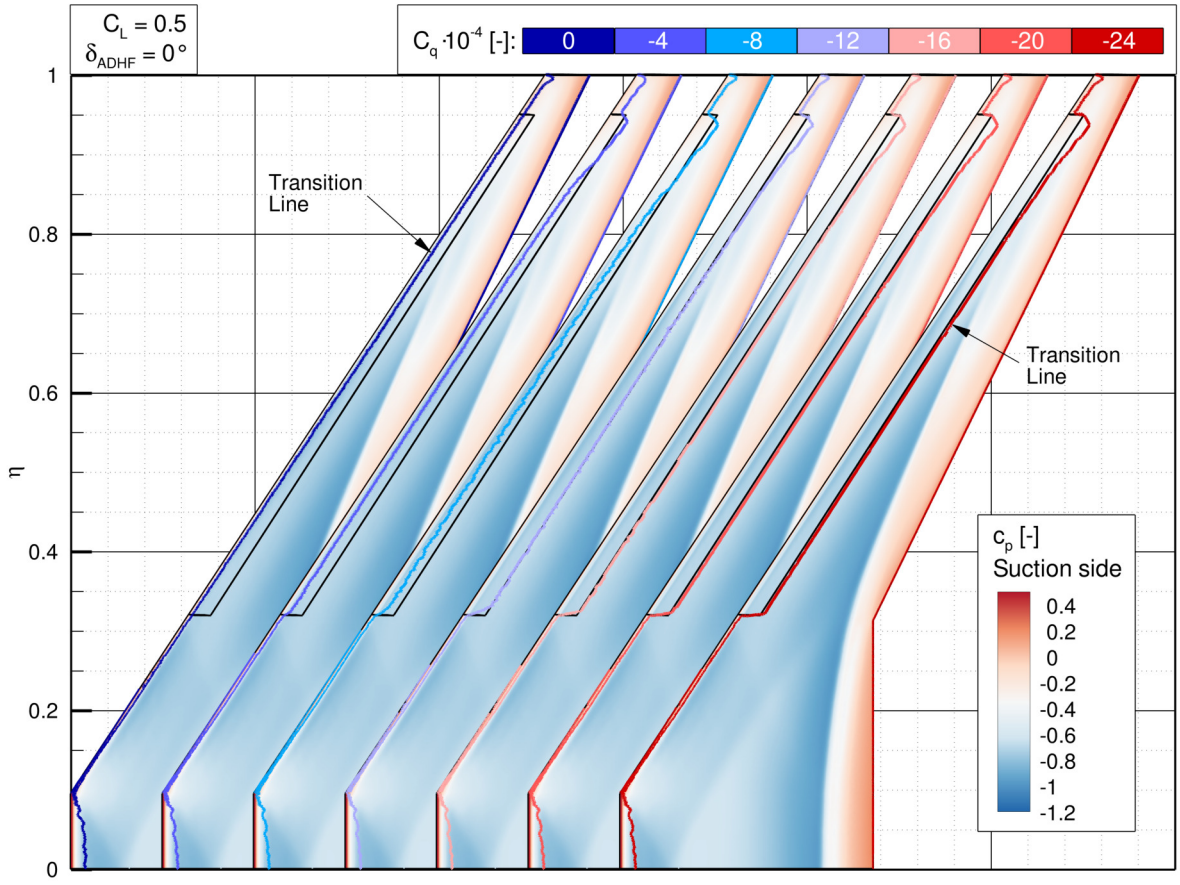

Figure 7 – Transition lines for $C_L = 0.5$, $\delta_{ADHF} = 0°$ with increasing magnitude of suction coefficient C_q. Additionally, pressure coefficient c_p contours on the wing's suction side are visualized.

effect on the wing skin friction coefficient $C_{d,f}$ is also minor, see Fig. 6. An increase in suction coefficient initially leads to a slight increase in skin friction drag, connected to higher local c_f levels due to reduced boundary layer thickness, see Fig. 6 d). The minimum level in skin friction drag is achieved for $C_q = 12 \cdot 10^{-4}$, corresponding to the combination of maximum downstream shift in transition location at the smallest suction strength C_q for the given geometry. A further increase in suction strength magnitude acts in further increasing $C_{d,f}$, since the transition location is not affected anymore.

4.2 Linear Stability Theory

The development of cross-flow and Tollmien-Schlichting N-factor envelopes for seven spanwise positions on the wing suction and pressure side are presented in Fig. 8. In addition, the different levels of critical N-factors, as indicated in Tab. 2, are incorporated to the figure.

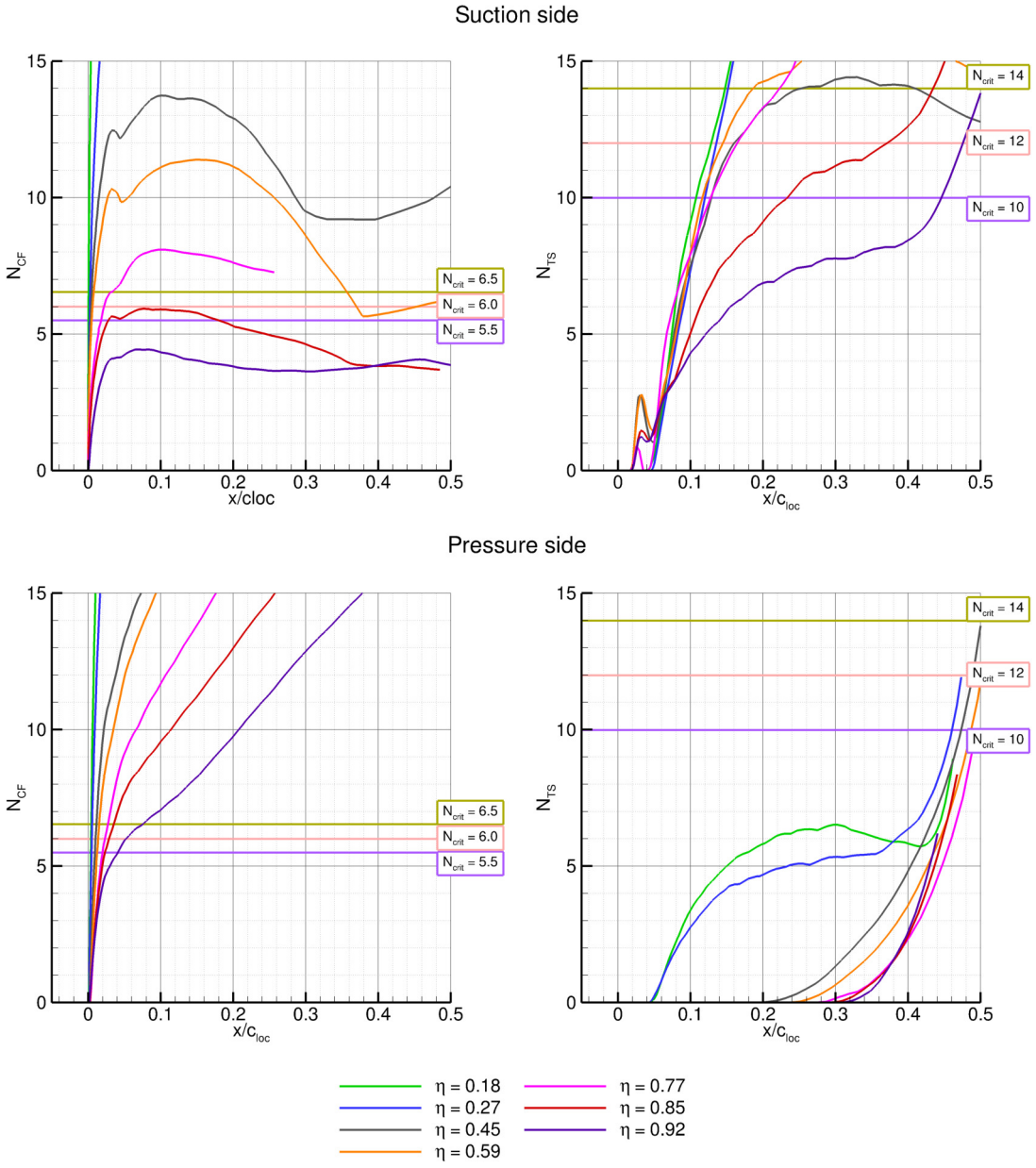

Figure 8 – N-factor development for cross-flow (CF) and Tollmien-Schlichting (TS) waves along the wing span for $\delta_{ADHF} = 0°$.

According to the chosen critical N-factors, transition is predicted due to cross-flow instabilities over the major part of the wing suction side and the entire span of the wing pressure side. Starting from the wing root, a strong amplification of cross-flow waves ($\eta = 0.18,\ 0.27$) leads to transition in direct vicinity of the wing's leading edge. Moving in outboard direction along the wing's span, the maximum in cross-flow amplification decreases, successively shifting the transition location downstream to a maximum chordwise position of $x_t/c_{loc} = [0.05; 0.09]$ with respect to the different critical N-factors for the wing pressure side. Considering the wing suction side, cross-flow N-factors fall below all critical levels between $\eta = 0.85$ and $\eta = 0.95$, predicting a shift in transition mechanism to critical amplifica-

tion of Tollmien-Schlichting waves, see also Fig. 10 for an overview of the transition front.
Application of the two-N-factor strategy for transition prediction allows for direct insights into interaction effects between the shaping of the wing surface pressure distribution through VC integration and the delay of boundary layer transition. N-factor envelopes for ADHF deflection angles of $\delta_{ADHF} = 0°$, $2°$ and $4°$ within the ADHF span and corresponding pressure coefficient distributions are presented in Fig. 9.

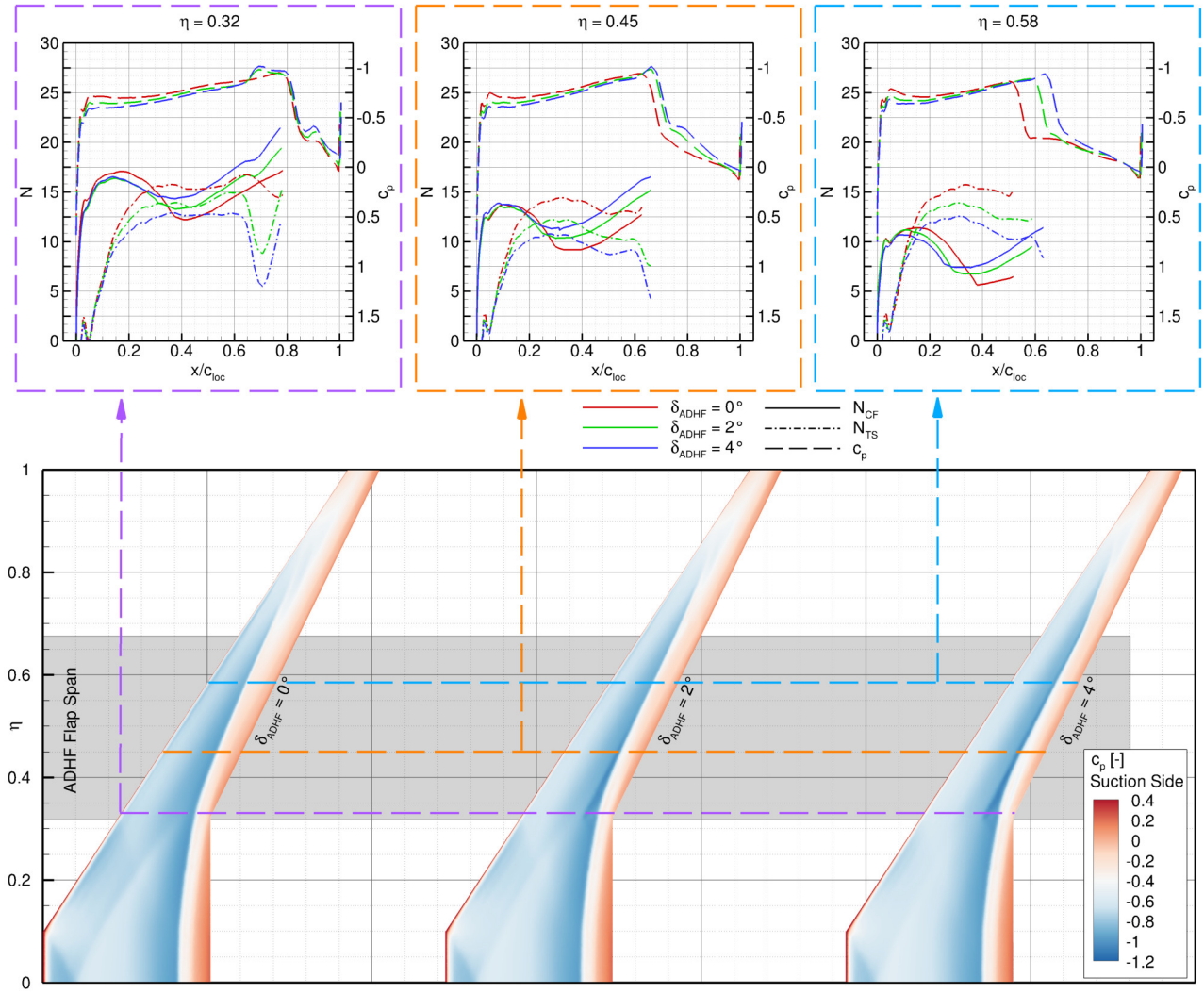

Figure 9 – N-factor development for cross-flow (CF) and Tollmien-Schlichting (TS) waves along the wing span for $\delta_{ADHF} = 0°$.

Increasing the ADHF deflection angle δ_{ADHF} generally leads to a downstream shift in shock location within the ADHF's span, aligning the shock front with the wing's trailing edge. The critical amplification of cross-flow waves at the wing leading edge is not influenced by altering the ADHF deflection angle, while generally higher cross-flow amplification rates are observable surpassing $x/c_{loc} \approx 0.3$. This behaviour is to be expected, since ADHF deflections in general increase the magnitude and chordwise extent of negative pressure gradient flow, thus underlining the necessity of an active suction system for supression of cross-flow instabilities.
In contrast, the adaptation in pressure distribution leads to the desired effect on amplification rates of Tollmien-Schlichting waves, namely a strong reduction in amplitude with increasing ADHF deflection angle δ_{ADHF}.
Considering ADHF deflection angles of $\delta_{ADHF} = 4°$, subcritical N-factors are achieved for all presented sections below the highest critical N-factor of $N_{TS,crit} = 14$. Suppression below the more conservative critical N-factor of $N_{TS,crit} = 12$ is achieved at $\eta = 0.45$.
ADHF deflection angles of $\delta_{ADHF} = 2°$ show a corresponding behaviour; intersection with the critical

N-factor of $N_{TS,crit} = 14$ is shifted from $x/c_{loc} \approx 0.22$ for the baseline wing to $x/c_{loc} \approx 0.5$ for $\delta_{ADHF} = 2°$ at $\eta = 0.32$. At the remaining spanwise sections N-factors do not surpass $N_{TS,crit} = 14$, while amplification rates stay below $N_{TS,crit} = 12$ at $\eta = 0.45$.

4.3 Comparison of predicted transition locations

As a final analysis, a comparison between the predicted transition locations for the no suction cases adopting both the turbulence modelling framework and the two-N-factor LST method for representative spanwise sections is given in Fig. 10.

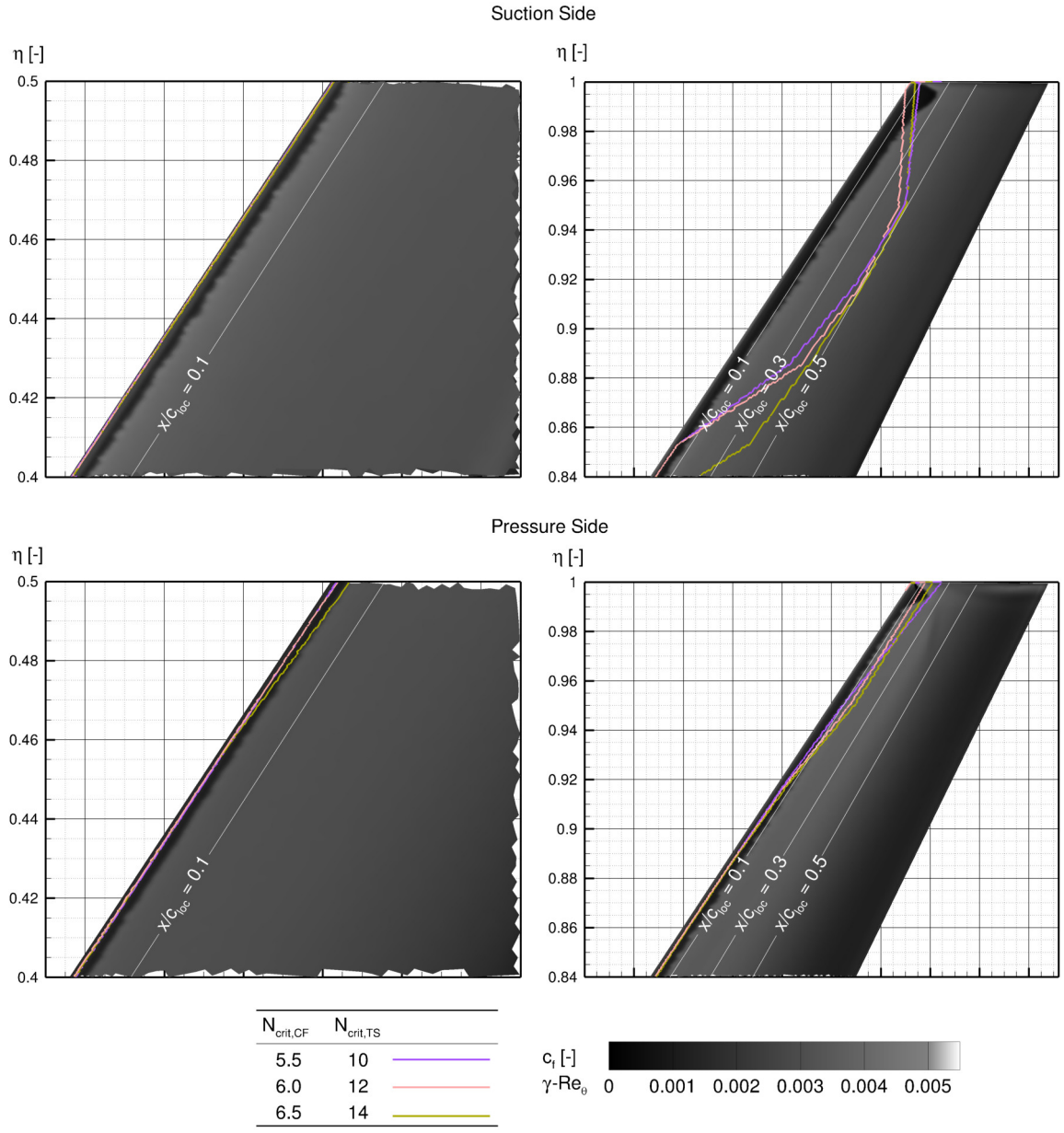

Figure 10 – Comparison of predicted transition locations at $\delta_{ADHF} = 2°$ for representative spanwise sections on the wing suction (top) and pressure (bottom) sides. The contour shows the distribution of skin friction coefficient computed via the $\gamma - Re_\theta + CF$ transition turbulence model, along with transition lines predicted via LST with the two-N-factor method according to the different critical N-factors from Tab. 2.

As described above, transition in direct vicinity of the wing's leading edge characterizes the analyses with the $\gamma - Re_\theta + CF$ model. Considering the wing's suction side, this is in line with the predicted tran-

sition mechanism by the two-N-factor method up to a spanwise position of $\eta = 0.82$ for $N_{crit,CF} = 6.5$ and $\eta = 0.855$ for $N_{crit,CF} = 5.5$ and 6.0, where the two-N-factor method predicts a shift in transition mechanism to critical TS-wave amplification. In the CF amplification region, transition prediction with the two-N-factor method shows little sensitivity to the chosen critical N-factors, the transition location is predicted upstream of the $\gamma - Re_\theta + CF$ counterpart.
With respect to the wing's pressure side, transition is attributed to CFI over the entire wing span. Again, the sensitivity to different critical N-factors is little, due to the high gradient and maximum value in CF N-factors computed in the wing's leading edge region, see Fig. 8. A slight downstream shift in transition lines predicted by the two-N-factor method is observable for $\eta > 0.92$, matching the transition location of its $\gamma - Re_\theta + CF$ equivalent best for a critical cross-flow N-factor of $N_{crit,CF} = 5.5$.
As for the wing suction side, the transition position is generally predicted upstream with regard to the position of the $\gamma - Re_\theta + CF$ model. Nevertheless, the differences in predicted transition location between both methods is smaller on the wing's pressure side than on the suction side.
As a final remark, the choice of critical N-factors is prone to uncertainty. While recommendations are given in the literature, calibration is typically performed following experimental results, which are not available for the present case. In case of cross-flow amplification of the no suction case, the configuration CATeW-02 is rather insensitive to the choice of critical N-factors due to the high amplification rates predicted in the wing's leading edge region. This is different for amplification rates of Tollmien-Schlichting waves, where transition location might scatter more markedly with respect to the chosen critical N-factors. Another uncertainty in critical N-factors might be introduced for the suction cases, for which further assessments incorporating a broader range of critical N-factors, especially for the non-zero suction cases, will be performed. LST presents an indispensable complementary tool to the transition prediction based on the $\gamma - Re_\theta + CF$, providing quantifiable physical insight into the critical transition mechanisms and opening the opportunity for calibration and to some extent validation of the $\gamma - Re_\theta + CF$ model.

5. Conclusions and Outlook

Within this contribution, computational fluid dynamics (CFD) results of the transitional flow around a transonic transport aircraft wing incorporating a hybrid laminar flow control (HLFC) system and variable camber (VC) capability by means of Adaptive Dropped Hinge Flap (ADHF) deflections are presented. The framework for the analyses is formed by the LuFo VI-1 project CATeW (*Coupled Aerodynamic Technologies for Aircraft Wings*), which shall assess synergy effects between the coupled HLFC-VC application with respect to drag reduction.
To conduct the analyses, different implementations for the CFD-framework (DLR TAU Code) have been performed in the course of the project. These are introduced within the paper, featuring modelling of the HLFC system through an adapted mass-flux boundary condition for application of user-defined suction velocity surface distributions, and usage of the DLR TAU code's mesh deformation capabilities to reflect different ADHF deflection settings.
To include the effects of boundary layer transition to the analyses, the $\gamma - Re_\theta + CF$ model is applied on the one hand, and linear stability theory (LST) coupled to a two-N-factor transition prediction method on the other hand. Computations applying the $\gamma - Re_\theta + CF$ model under variation of both the HLFC system's suction strength and the ADHF deflection angle, assess a maximum drag reduction for a suction strength of $C_q = -16 \cdot 10^{-4}$ and $\delta_{ADHF} = 2°$. The transition location is shifted downstream with increasing suction strength, nevertheless reaching its largest extent at the downstream limit of the HLFC suction panel for $C_q = -12 \cdot 10^{-4}$. A further increase in suction strength is not affecting the predicted transition location.
To complement the analyses with the $\gamma - Re_\theta + CF$ model and gain quantitative physical insight into dominant transition mechanisms, a first set of analyses applying LST with a two-N-factor transition prediction method for different critical N-factors is presented in the paper. The computations are performed for the no suction case, where, as for the $\gamma - Re_\theta + CF$ model, transition is predicted immediately at the wing's leading edge due to strong amplification of cross-flow waves. This behaviour is observed on the entire pressure side of the wing, the suction side (in the most conservative case of $N_{crit,CF} = 5.5$) features a region of subcritical cross-flow amplification for $\eta > 0.855$, altering the

transition mechanism to critical amplification of Tollmien-Schlichting instabilities. In case of critical cross-flow wave amplification, LST shows an upstream shift in predicted transition location when compared to the $\gamma - Re_\theta + CF$ model.
One of the central envisaged synergy effects of the technology coupling is enhancing the natural laminar flow extent of the HLFC wing using the wing's VC capability for favorable shaping of the pressure distribution. Applying the two-N-factor transition prediction method, studies are presented within this contribution focusing on the amplification rates of Tollmien-Schlichting waves under varying ADHF deflection angles. Adapting the deflection angle results in a pronounced reduction of Tollmien-Schlichting wave N-factors, corroborating the potential for synergetic application of the technology coupling to a transonic transport aircraft wing.

Contact Author Email Address

mailto: mauricio.jentys@tum.de

Acknowledgments

The funding of the presented investigations within the LuFo VI-1 project CATeW (Coupled Aerodynamic Technologies for Aircraft Wings, FKZ: 20E1917B) by the German Federal Ministry for Economic Affairs and Climate Action (BMWK) is gratefully acknowledged. Furthermore, the authors deeply appreciate the German Aerospace Center (DLR) for providing the DLR TAU Code used for the numerical HiFi - investigations. Moreover, the authors would like to thank the Gauss Centre for Supercomputing e.V. (www.gauss-centre.eu) for providing computing time on the GCS Supercomputer SuperMUC-NG at Leibniz Supercomputing Center (LRZ, www.lrz.de).

Copyright Statement

References

[1] European Commission and Directorate-General for Mobility and Transport and Directorate-General for Research and Innovation Flightpath 2050: Europe's Vision for Aviation : Maintaining Global Leadership and Serving Society's Needs. Publications Office (2011). https://doi.org/10.2777/5026

[2] Joslin, R. D. Overview of Laminar Flow Control: Technical Report (1998)

[3] Krishnan, K. S. G., Bertram, O. , Seibel, O. Review of hybrid laminar flow control systems. *Progress in Aerospace Sciences* 93, 24–52 (2017). https://doi.org/10.1016/j.paerosci.2017.05.005

[4] Szodruch, J. The Influence of Camber Variation on the aerodynamics of Civil Transport Aircraft. In: American Institute of Aeronautics and Astronautics (ed.) *AIAA 23st Aerospace Sciences Meeting* (1985). https://doi.org/10.2514/6.1985-353

[5] Bolokin, A. , Gilyard, G. B. Estimated Benefits of Variable-Geometry Wing Camber Control for Transport Aircraft (1999)

[6] Risse, K. , Anton, E. , Lammering, T. , Franz, K. , Hoernschemeyer, R. An Integrated Environment for Preliminary Aircraft Design and Optimization. In: American Institute of Aeronautics and Astronautics (ed.) *53rd AIAA/ASME/ASCE/AHS/ASC Structures, Structural Dynamics and Materials Conference: SciTech 2012*, vol. AIAA 2012-1675 (2012). https://doi.org/10.2514/6.2012-1675

[7] Schueltke, F. , Aigner, B. , Effing, T. , Strathoff, P. , Stumpf, E. MICADO: Overview of Recent Developments within the Conceptual Aircraft Design and Optimization Environment. In: Deutsche Gesellschaft für Luft- und Raumfahrt - Lilienthal - Oberth e.V. (ed.) *69. Deutscher Luft- und Raumfahrtkongress* (2020). https://doi.org/10.25967/530093

[8] Effing, T. , Schmitz, V. , Schueltke, F. , Peter, F. , Stumpf, E. Combined application of hybrid laminar flow control and variable camber in preliminary aircraft design. In: *33rd Congress of the International Council of the Aeronautical Sciences*. accepted for presentation and publication, Stockholm, Sweden (2022)

[9] Schlichting, H. , Gersten, K. *Boundary-Layer Theory*. Springer Berlin Heidelberg, Berlin, Heidelberg (2017). https://doi.org/10.1007/978-3-662-52919-5

[10] Beck, N. , Landa, T. , Seitz, A. , Boermans, L. , Liu, Y. , Radespiel, R. Drag reduction by laminar flow control. *Energies* 11(252), 1–28 (2018). https://doi.org/10.3390/en11010252

[11] Saric, W. S., Reed, H. L., White, E. B. Stability and transition of three-dimensional boundary layers. *Annual Review of Fluid Mechanics* 35(1), 413–440 (2003). https://doi.org/10.1146/annurev.fluid.35.101101.161045

[12] Tollmien, W. Ein Allgemeines Kriterium der Instabilität Laminarer Geschwindigkeitsverteilungen. Nachrichten von der Gesellschaft der Wissenschaften zu Göttingen, Mathematisch-Physische Klasse. Weidmann (1935)

[13] Pfenninger, W. Some Results from the X-21A Programm. Part I: Flow Phenomena at the Leading Edge of Swept Wings. *Recent Developments in Boundary Layer Research, AGARDograph* 97(4), 1–41 (1965)

[14] Poll, D. I. A. Transition in the infinite swept attachment line boundary layer. *Aeronautical Quarterly* 30(4), 607–629 (1979). https://doi.org/10.1017/S0001925900008763

[15] Peter, F. N., Risse, K. , Schueltke, F. , Stumpf, E. Variable camber impact on aircraft mission planning. In: American Institute of Aeronautics and Astronautics (ed.) *53rd AIAA Aerospace Sciences Meeting 2015*, vol. AIAA 2015-1902. Curran, Red Hook, NY (2015). https://doi.org/10.2514/6.2015-1902

[16] Schwamborn, D. , Gardner, A. , von Geyer, H. , Krumbein, A. , Lüdeke, H. , Stürmer, A. Development of the TAU-Code for aerospace applications. In: *50th NAL International Conference on Aerospace Science and Technology* (2008)

[17] Woehler, S. , Hartmann, J. , Prenzel, E. , Kwik, H. Preliminary aircraft design for a midrange reference aircraft taking advanced technologies into account as part of the AVACON project for an entry into service in 2028. In: Deutsche Gesellschaft für Luft- und Raumfahrt - Lilienthal - Oberth e.V. (ed.) *67. Deutscher Luft- und Raumfahrtkongress* (2018). https://doi.org/10.25967/480224

[18] Jentys, M. , Effing, T. , Breitsamter, C. , Stumpf, E. Numerical Analyses of a Reference Wing for Combination of Hybrid Laminar Flow Control and Variable Camber. CEAS Aeronautical Journal (2022, submitted for publication)

[19] Strüber, H. The Aerodynamic Design of the A350 XWB-900 High Lift System. In: International Council of the Aeronautical Sciences (ed.) *29th International Congress of the Aeronautical Sciences* (2014)

[20] Reckzeh, D. Der intelligente Tragflügel: Multifunktionale Klappen an der A350 XWB und der Weg zu zukünftigen Konzepten. Luft- und Raumfahrt (1), 22–25 (2018)

[21] Nie, S. Extension of transition modeling by a transport equation approach. Technical report, DLR (2017). https://elib.dlr.de/113724/

[22] Fehrs, M. Boundary Layer Suction Modeling Based on the DLR TAU-Code Effusion Mass Flux Boundary Condition. In: Dillmann, A. , Heller, G. , Krämer, E. , Wagner, C. , Tropea, C. , Jakirlić, S. (eds.) *New Results in Numerical and Experimental Fluid Mechanics XII*, pp. 175–184. Springer International Publishing, Cham (2020). https://doi.org/10.1007/978-3-030-25253-3_17

[23] Krimmelbein, N. , Krumbein, A. Transition prediction for flows with suction using the e^N-method. https://doi.org/10.2514/6.2021-0630

[24] Grabe, C. , Shengyang, N. , Krumbein, A. Transport Modeling for the Prediction of Crossflow Transition. *AIAA Journal* 56(8), 3167–3178 (2018). https://doi.org/10.2514/1.J056200

[25] Langtry, R. B., Menter, F. R. Correlation-Based Transition Modeling for Unstructured Parallelized Computational Fluid Dynamics Codes. *AIAA Journal* 47(12), 2894–2906 (2009). https://doi.org/10.2514/1.42362

[26] Menter, F. R. Two-equation eddy-viscosity turbulence models for engineering applications. *AIAA Journal* 32(8), 1598–1605 (1994). https://doi.org/10.2514/3.12149

[27] Schrauf, G. LILO 2.1: User's Guide and Tutorial: GSSC Technical Report 6 (2006)

[28] Schrauf, G. COCO: A Program to Compute Velocity and Temperature Profiles for Local and Nonlocal Stability Analysis of Compressible, Conical Boundary Layers with Suction: Technical Report ZARM, Bremen (1998)

[29] Krumbein, A. , Krimmelbein, N. , Schrauf, G. Automatic Transition Prediction in Hybrid Flow Solver, Part 1: Methodology and Sensitivities. *Journal of Aircraft* 46(4), 1176–1190 (2009). https://doi.org/10.2514/1.39736

[30] Lynde, M. N., Campbell, R. L. *Computational Design and Analysis of a Transonic Natural Laminar Flow Wing for a Wind Tunnel Model*, (2017). https://doi.org/10.2514/6.2017-3058